frontiers | Frontiers in Earth Science

TYPE Original Research
PUBLISHED 07 June 2024
DOI 10.3389/feart.2024.1366213

OPEN ACCESS

EDITED BY
Marco Viccaro,
University of Catania, Italy

REVIEWED BY
Roberto Moretti,
UMR7154 Institut de Physique du Globe de Paris (IPGP), France
Yuri Taran,
National Autonomous University of Mexico, Mexico

*CORRESPONDENCE
Alexis Bernard,
alexis.bernard@univ-pau.fr

RECEIVED 05 January 2024
ACCEPTED 10 April 2024
PUBLISHED 07 June 2024

CITATION
Bernard A, Battani A, Rizzo AL, Balci U, Györe D, D'Alessandro W, Callot J-P, Kyriakopoulos K and Pujol M (2024), Temporal monitoring of fumarole composition at Santorini volcano (Greece) highlights a quiescent state after the 2011–2012 unrest. *Front. Earth Sci.* 12:1366213. doi: 10.3389/feart.2024.1366213

Temporal monitoring of fumarole composition at Santorini volcano (Greece) highlights a quiescent state after the 2011–2012 unrest

Alexis Bernard[1]*, Anne Battani[1], Andrea Luca Rizzo[2,3], Uğur Balci[4], Domokos Györe[4,5], Walter D'Alessandro[6], Jean-Paul Callot[1], Konstantinos Kyriakopoulos[7] and Magali Pujol[8]

[1]Laboratoire des Fluides Complexes et leurs Réservoirs (LFCR), Université de Pau et des Pays de l'Adour (UPPA), Pau, France, [2]Department of Earth and Environmental Sciences, University of Milano-Bicocca, Milan, Italy, [3]Istituto Nazionale di Geofisica e Vulcanologia (INGV), Sezione di Milano, Milano, Italy, [4]Scottish Universities Environmental Research Centre (SUERC), East Kilbride, United Kingdom, [5]Isomass Scientific Inc., Calgary, AB, Canada, [6]Istituto Nazionale di Geofisica e Vulcanologia (INGV), Sezione di Palermo, Palermo, Italy, [7]Department of Geology and Geoenvironment, National and Kapodistrian University of Athens, Athens, Greece, [8]TotalEnergies/OneTech, Pau, France

Santorini Island (Greece) is an active volcano which has alternated between dormant and active periods over the last 650,000 years with the latest volcanic unrest occurring in 2011–2012. Here we report a geochemical survey of fumarolic gases collected at Nea Kameni islet located in the center of the caldera over the period 2015–2022 in order to study the activity of the volcano and changes in hydrothermal conditions. This period is marked by the absence of significant geochemical anomalies compared to the unrest of 2011–2012, implying that no new magma upwelling has occurred. This is evident from the low CO_2/CH_4 ratio and H_2 concentration of fumaroles. An increase of the atmospheric contribution in gases after the 2011–2012 unrest suggests a decrease of the deep gas flow and the chemical and C-He-isotope compositions are compatible with a model of Rayleigh fractionation in which CO_2 dissolves in water at decreasing temperatures over time. These results are consistent with temperature estimates obtained using the H_2/N_2 geothermometer, seismic and geodetic evidences. This implies a slowing of the degassing of the hydrothermal/volcanic system and a cooling of the magma injected at shallow depth in 2011–2012. All these conclusions support a quiescent state of the Santorini volcano over the period 2015–2022.

KEYWORDS

Santorini, volcano monitoring, fumarole geochemistry, He isotope composition, gas-water interaction

1 Introduction

Santorini Island (Greece) is one of the most active and dangerous volcanic systems of the South Aegean Active Volcanic Arc (SAAVA). The volcano has been active subaerially for at least 650,000 years and volcanic activity follows a broadly cyclic behavior; 1. Plinian/explosive eruption, 2. inter-Plinian/effusive edifice construction and 3. quiescence. These cycles typically last 10,000–30,000 years (Druitt et al., 2019). During the last

350,000 years Santorini has experienced twelve explosive eruptions and at least four caldera collapses (Druitt et al., 1999). The last Plinian eruption, referred to as the "Minoan", occurred in the Late Bronze Age (LBA) (~3,600 years ago) and caused catastrophic damage across the southern Aegean (Bond and Sparks, 1976). Since then the volcano has exhibited effusive dacitic activity with the most recent eruption occurred in 1950 at Nea Kameni, in the center of the caldera (Georgalas, 1953). After 60 years of quiescence Santorini experienced intense seismic-geodetic-geochemical unrest in 2011–2012. This has been interpreted as a response to new magma intrusion into the shallow plumbing system (Newman et al., 2012; Parks et al., 2012; Papoutsis et al., 2013; Tassi et al., 2013; Rizzo et al., 2015). Although no eruption occurred, the volcanic hazard remains.

Knowledge of the dynamics of magma recharge in quiescent volcanoes is essential for addressing the issues related to volcanic hazards (Rosi et al., 2022). In this respect, the study and temporal monitoring of volcanic/hydrothermal gases revealed helpful in evaluating the volcano state of activity and the evolution of these signatures can help understand the magmatic processes occurring at depth, such as magma upwelling or crustal assimilation (Caracausi et al., 2003; Chiodini, 2009; Caliro et al., 2014; Torres-González et al., 2020). In this work, we combine a new set of gas geochemistry data that cover the period 2015–2022, with published pre-2015 data to study the temporal evolution of the chemical and C-He-isotope compositions of the gas from a single fumarole at Nea Kameni. We use these data to monitor the state of the volcanic system and study its influence on the hydrothermal system.

1.1 Geologic setting and volcanological background

Since the closure of the Tethyan Ocean at the end of the Cretaceous, the convergence between Africa and Europe has generated complex geodynamics in the Aegean domain (Jolivet and Brun, 2010; Jolivet et al., 2013). The SAAVA (Figure 1) is a 500 km long curved chain of active Upper Pliocene-Quaternary volcanoes, which extends from Greece to Turkey (Fytikas et al., 1984). It results from the northward subduction of the African plate (oceanic crust remnant) beneath Eurasia (continental Aegean microplate), with the current convergent plate boundary (i.e., Ionian trench) located south of Crete (Le Pichon and Angelier, 1979). The southward slab retreat caused back arc extension and slab segmentation in the Aegean and Anatolian domains (Piromallo and Morelli, 2003; Biryol et al., 2011; Jolivet et al., 2013; Jolivet et al., 2015; Sachpazi et al., 2016; Bocchini et al., 2018; Hansen et al., 2019). The Aegean arc is characterized by calc-alkaline to high-K calc-alkaline volcanism, with rock compositions that evolve from basalts to rhyolites developed on thinned (20–22 km thick) continental crust (Francalanci et al., 2005; Grigoriadis et al., 2016). Santorini is located in the central part of the arc and belongs to the NE-SW oriented Christiana-Santorini-Kolumbo Volcanic Field (i.e., CSKVF), an alignement of volcanoes that extends from Christiana in the southwest to numerous small submarine volcanoes in the northeast (~70 km) (Figure 2A) (Nomikou et al., 2019; Preine et al., 2021). The position and orientation of the CSKVF are strongly controlled by the extensional tectonic regime of the Santorini-Amorgos Tectonic Zone (i.e., SATZ), comprising NE-SW oriented active faults and sedimentary basins (Bohnhoff et al., 2006; Nomikou et al., 2018).

The Santorini archipelago is composed of five islands: Thera, Therasia and Aspronisi form the walls of the caldera and are the remains of the pre-LBA volcanic activity, whereas Nea Kameni and Palea Kameni (i.e., NK and PK) in the center of the caldera postdate the Minoan caldera-forming eruption (Figure 2B) (Fouqué, 1879; Druitt et al., 1999; Pyle and Elliott, 2006; Nomikou et al., 2014). The Meso-Cenozoic pre-volcanic basement of Santorini is mainly composed of limestones, marbles and metapelites metamorphosed up to the blueschist grade (Druitt et al., 1999; Lion, 2018 and reference therein). These rocks are exposed in the southeast part of Thera and inferred at ~1.5 km depth below Nea Kameni (Budetta et al., 1984). The volcano-tectonic activity is concentrated along two major NE-SW structures (Nea Kameni and Kolumbo lines) showing different seismic behavior (Barberi and Carapezza, 1994; Pfeiffer, 2001; Dimitriadis et al., 2009; Stiros et al., 2010; Parks et al., 2012; Heath et al., 2019; bbnet.gein.noa.gr). The parental magmas of Santorini are generated by high degrees of partial melting of an Aegean depleted mantle wedge (ADM) that has been metasomatized by slab sediments and aqueous fluids (Francalanci and Zellmer, 2019 and references therein; Flaherty et al., 2022). The mantle source also reflects a contribution of sub-slab enriched mantle (SSEM) that may have upwelled through a tear beneath Anatolia in the down-going African plate (Klaver et al., 2016). During their ascent, magmas evolve by fractional crystallization and crustal assimilation, magma mixing and mingling phenomena (Druitt et al., 2019 and references therein; Pank et al., 2022). The submarine volcano of Kolumbo, located ~7 km northeast of Santorini is considered as the most active volcanic system of the region and despite the strong geographical and tectonic links between Santorini and Kolumbo, these volcanic systems are characterized by significant geochemical and seismic contrasts. This is evident for instance from the higher He isotopic ratios measured in the gas emissions of Kolumbo (Carey et al., 2013; Rizzo et al., 2016; 2019) or inferred from geochemical and seismic data (Dimitriadis et al., 2009; 2010; Cantner et al., 2014; Klaver et al., 2016; Nomikou et al., 2019 and references therein). These contrasted behaviours seem to relate differences in the plumbing systems rather than a variability of magmatic sources and an asthenosphere mantle with $^{3}He/^{4}He$ of at least 7 R_a has been proposed for both volcanoes (Rizzo et al., 2016). Nevertheless, the possibility of local mantle heterogeneity is still being debated (Klaver et al., 2016).

1.2 The 2011–2012 Santorini unrest

After the eruption in 1950, Santorini has been in a quiescent state characterized by gas released at fumaroles and bubbling springs mostly at the Nea Kameni and Palea Kameni islets. In 2011, GPS and InSAR data highlighted a significant ground inflation, accompanied by a seismic swarm at shallow depth (<6 km) within the caldera (Newman et al., 2012; Papageorgiou et al., 2012; Parks et al., 2012; Papoutsis et al., 2013). This implied that the Kameni line had been reactivated (Feuillet, 2013). Changes in the composition of fumarolic

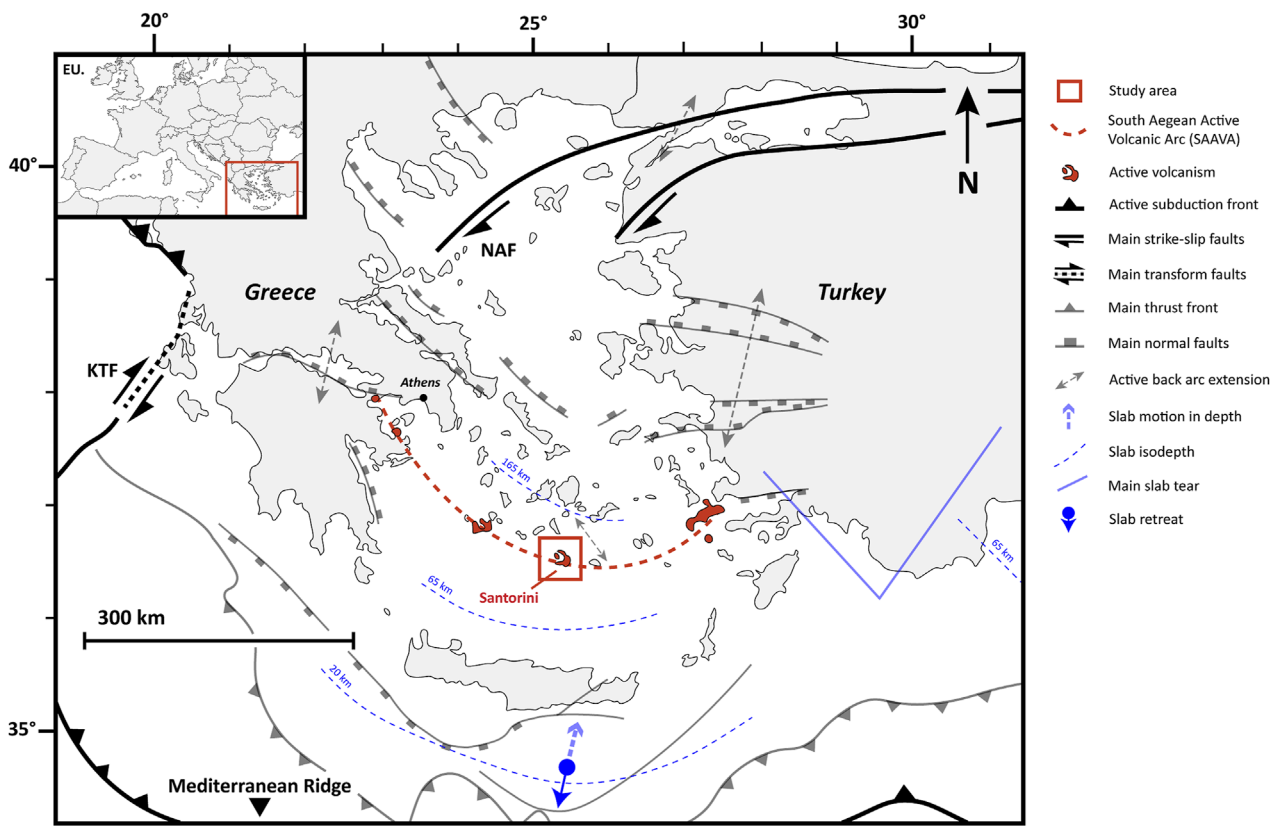

FIGURE 1
Tectonic map of the Aegean Sea showing the location of Santorini. Slab features are also reported. KTF: Kephalonia Transform Fault. NAF: North Anatolian Fault. Modified from Jolivet et al., 2013.

gas and condensates and soil CO_2 flux have been measured at Nea Kameni since 2011. Increases in the CO_2/CH_4, N_2/Ar and the diffusive emission rate of CO_2 have been interpreted as an input of deep volatiles into the hydrothermal system (Parks et al., 2013; Tassi et al., 2013; Rizzo et al., 2015). A sharp increase in the H_2 concentration was attributed to the thermal dissociation of H_2O due to the heat pulse from the new magmatic body (Tassi et al., 2013). The increase of hydrothermal temperature to 275°C has been proposed on the basis of CO/CO_2 and H_2/N_2 gas geothermometers (Tarchini et al., 2019). An increase in the He isotopic ratio (Rizzo et al., 2015) has been attributed to upwelling of fresh volatile-rich magma (~16 x 10^6 m^3) to a depth of ~4 km between Nea Kameni and Therasia (Figure 2B) (Newman et al., 2012; Papageorgiou et al., 2012; Parks et al., 2012; 2015; Lagios et al., 2013; Papoutsis et al., 2013; Papadimitriou et al., 2015; Rizzo et al., 2015). These changes led to the fear of an imminent eruption because mafic magma input can trigger effusive eruption on short time scales (e.g., in less than 1-month) (Martin et al., 2008) whereas Plinian eruptions can result from several recharges of a silicic magma reservoir in less than 100 years (Druitt et al., 2012). Both seismic activity and the ground deformation increased progressively until 2012. This unrest was not followed by eruption and gas compositions returned to levels observed before the unrest (Rizzo et al., 2015; Bountzouklis, 2016; Papageorgiou et al., 2019; Tarchini et al., 2019).

1.3 Sampling and analytical techniques

Gas samples were collected from fumaroles located in the center of the Nea Kameni islet (Figure 2B). These fumaroles are characterized by weak gas emissions fed by a shallow hydrothermal system and undergoing in-soil steam condensation together with air contamination before reaching the surface. The low gas temperatures measured at the vent discharges (~90°C) appear to be constant over the years despite the temporal changes of the hydrothermal temperature evidenced by the geothermometers (Tarchini et al., 2019). Previous monitoring of fumarolic gases have been carried out at the same sampling sites using a similar method (Nagao et al., 1991; Chiodini, 1998; Shimizu et al., 2005; D'Alessandro et al., 2010; Tassi et al., 2013; Rizzo et al., 2015; Daskalopoulou, 2017; Tarchini et al., 2019). Eight batches of sample were collected by the INGV, Sezione di Palermo (Italy), from a fumarole of reference denoted by NK over the period of 2015–2022 at a frequency of about one sample per year (Table 1; Figure 2C). For chemical and C-isotopic measurements ($\delta^{13}C$-CO_2), two-way Pyrex bottles with vacuum valves were used to store the collected gases. Noble gas samples were collected in stainless steel tubes equipped with all-metal Swagelok valves. Three batches of sample were collected in January 2022 by the LFCR (Pau, France) from three different fumaroles denoted by Nea 1, Nea 2, and Nea 3 (Table 1; Figure 2C). Vacutainers were used for major gas and carbon isotope samples and

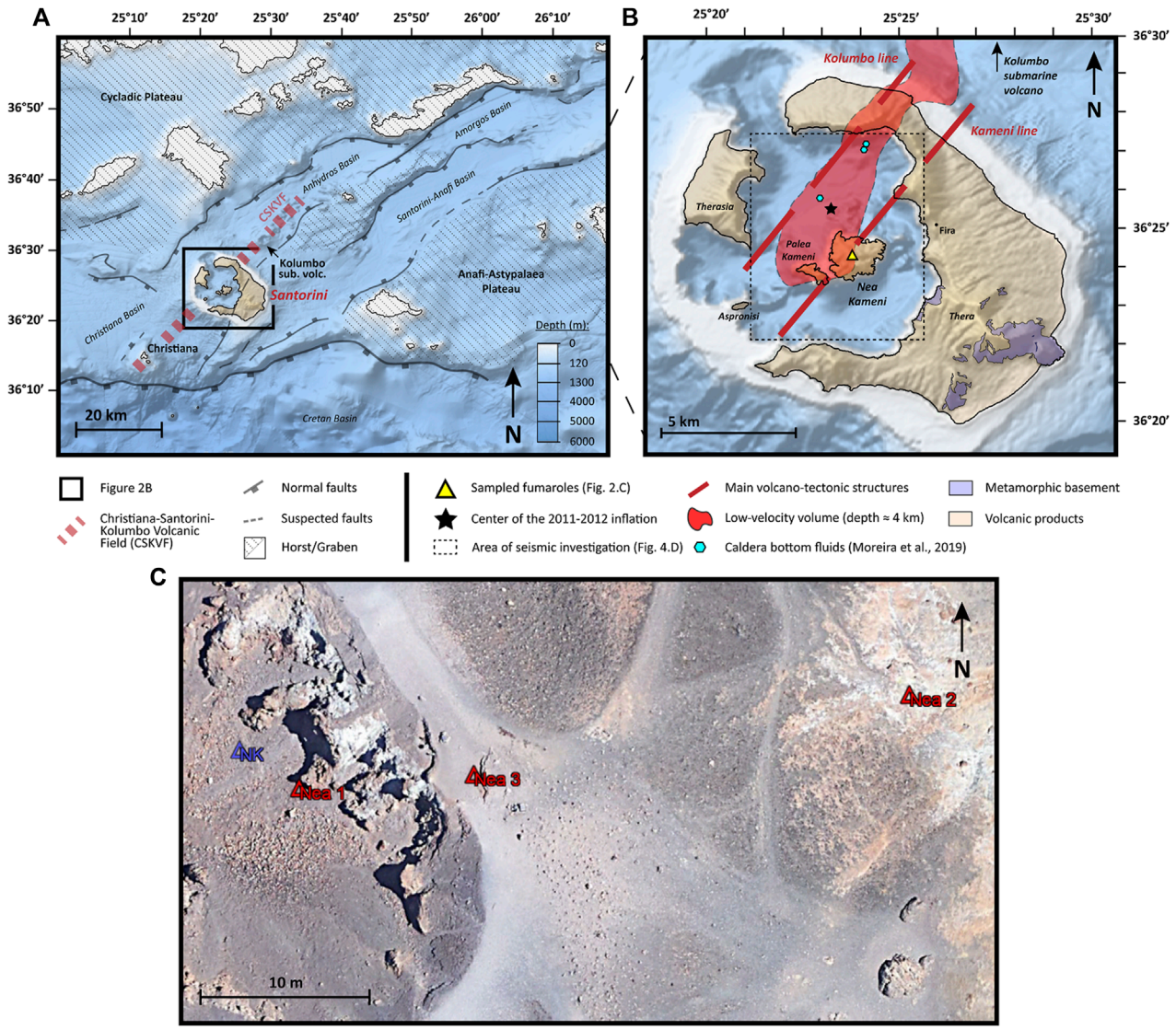

FIGURE 2
(A) Simplified tectonic map of the Santorini-Amorgos Tectonic Zone (SATZ). The location of the Christiana-Santorini-Kolumbo Volcanic Field (CSKVF) is also reported. Bathymetry data come from EMODNET database (www.emodnet.eu). Modified from Nomikou et al., 2018. **(B)** Simplified geological map of Santorini with the main volcano-tectonic lines, emplacement of the magmatic body in depth and samples location. Modified from Druitt et al., 1989; Parks et al., 2012; Heath et al., 2019; McVey et al., 2020. The dashed square corresponds to the area of investigation for the seismic monitoring of Figure 4D. **(C)** Location of the sampled fumaroles at Nea Kameni.

annealed copper tubes for noble gas samples. A batch of samples was generally composed by two to four samples for chemical and carbon isotope analysis and one for noble gas isotope analysis. The sampling was carried out by using an inverted funnel to channel the gas flow into the appropriate containers. The sampling system was flushed with fumarolic gases for several tens of minutes to minimize internal atmospheric contamination.

The samples collected from the NK fumarole were analyzed for chemical composition (N_2, O_2, CO_2, CH_4, H_2, H_2S) using a Perkin Elmer Clarus500 gas chromatograph equipped with TCD and FID detectors and argon carrier gas. Repeatability is typically <3% of the measured values. The carbon isotope composition of CO_2 ($\delta^{13}C$-CO_2) was determined by a Thermo Fischer Delta Plus XP mass spectrometer, coupled with a Thermo TRACE gas chromatograph and a Thermo GC/C III interface. The carrier gas was He and results are given with uncertainties of ±0.1‰ with respect to the V-PDB standard (Craig, 1957). The abundance of ^{4}He and ^{20}Ne, as well as He isotopic ratio were determined using a Thermo Fischer Helix SFT (for helium) and a Thermo Fischer Helix MC Plus (for neon) following standard procedures (Rizzo et al., 2015; 2016). For the ^{4}He and ^{20}Ne contents, uncertainties are ranging from 0.02% to 0.08% and from 0.01% to 0.02%, respectively. Uncertainties on the He isotopic ratios range from 0.5% to 1.5% (Paonita et al., 2012; Rizzo et al., 2015; 2016; Daskalopoulou et al., 2018).

Chemical and carbon isotope compositions of the LFCR samples were performed by Isolab (Neerijnen, Netherlands). Chemical compositions were measured by two Agilent 6890N/7890A/7890B gas chromatographs equipped with TCD and FID detectors, with

TABLE 1 Sample details and composition of fumarole gases from Nea Kameni.

ID	Sample	Source	Sampling date	Latitude	Longitude
1	NK	INGV *	18/02/2015	36°24′16.40″ N	25°23′45.09″ E
2	NK	INGV *	06/04/2016	36°24′16.40″ N	25°23′45.09″ E
3	NK	INGV *	13/06/2017	36°24′16.40″ N	25°23′45.09″ E
4	NK	INGV *	27/05/2018	36°24′16.40″ N	25°23′45.09″ E
5	NK	INGV *	24/08/2018	36°24′16.40″ N	25°23′45.09″ E
6	NK	INGV *	06/07/2019	36°24′16.40″ N	25°23′45.09″ E
7	NK	INGV *	13/02/2020	36°24′16.40″ N	25°23′45.09″ E
8	Nea 1	LFCR *	20/01/2022	36°24′16.26″ N	25°23′45.36″ E
9	Nea 2	LFCR *	21/01/2022	36°24′16.60″ N	25°23′48.12″ E
10	Nea 3	LFCR *	21/01/2022	36°24′16.31″ N	25°23′46.15″ E
11	NK	INGV *	16/07/2022	36°24′16.40″ N	25°23′45.09″ E
	Air	-	-	-	-
	ASSW[1]	-	-	-	-

CO_2 (%)	N_2 (%)	O_2 (%)	Ar (%)	H_2 (ppm)	CH_4 (ppm)	$\delta^{13}C$-CO_2 (‰ vs. PDB)
64.33	27.77	6.03	n.m.	10100	300	n.m.
52.64	36.75	8.36	n.m.	8,8105	264	0.3
49.96	37.69	8.53	n.m.	7,7489	252	n.m.
51.97	36.63	8.22	n.m.	6,6887	265	n.m.
49.60	39.78	9.18	n.m.	5,5952	253	n.m.
53.53	36.31	7.99	n.m.	2,2834	278	0.0
46.22	43.35	9.32	n.m.	5,5849	387	n.m.
25.30	58.80	15.20	0.72	529	129	0.8
6.67	72.80	19.60	0.89	b.d.l.	46	0.6
29.30	55.90	13.70	0.69	3,3860	174	0.8
41.52	47.95	10.60	n.m.	5,5825	230	n.m.
0.038	78.08	20.95	0.93	0.53	1.7	−8.0
1.4	62.60	34.30	1.59	-	3.8	-

$^3He/^4He$ (Ra)	Err. R/R[a] (+/−)	^4He (ppm)	Err. 4He (+/−)	$^4He/^{20}Ne$	Rc/Ra	CO_2/CH_4	$CO_2/^3He$
2.96	0.015	6.99	0.0017	1.09 ± 0.0005	3.77 ± 0.06	2,2144 ± 129	2.23E+10 ± 9.93E+08
2.65	0.023	6.02	0.0023	0.92 ± 0.0005	3.52 ± 0.07	1994 ± 120	2.36E+10 ± 1.14E+09
2.70	0.018	6.45	0.0024	1.12 ± 0.0006	3.38 ± 0.06	1983 ± 119	2.05E+10 ± 9.48E+08

(Continued on the following page)

TABLE 1 (*Continued*) Sample details and composition of fumarole gases from Nea Kameni.

$^3He/^4He$ (Ra)	Err. R/R[a] (+/−)	^4He (ppm)	Err. 4He (+/−)	$^4He/^{20}Ne$	Rc/Ra	CO_2/CH_4	$CO_2/^3He$
2.89	0.021	7.51	0.0020	1.09 ± 0.0004	3.67 ± 0.06	1961 ± 118	1.71E+10 ± 8.00E+08
2.84	0.021	7.09	0.0018	0.88 ± 0.0003	3.88 ± 0.07	1960 ± 118	1.76E+10 ± 8.27E+08
2.86	0.043	7.00	0.0023	0.96 ± 0.0004	3.78 ± 0.10	1926 ± 116	1.91E+10 ± 1.05E+09
2.32	0.029	8.54	0.0066	0.74 ± 0.0007	3.33 ± 0.08	1,1194 ± 72	1.67E+10 ± 8.82E+08
1.42	0.076	9.22	0.23	0.43 ± 0.0238	2.65 ± 0.46	1961 ± 78	1.38E+10 ± 1.49E+09
n.m.	n.m.	n.m.	n.m.	-	-	1,1450 ± 58	-
2.43	0.092	8.88	0.22	0.58 ± 0.0453	4.17 ± 0.85	1,1684 ± 67	9.70E+09 ± 8.91E+08
2.43	0.032	5.98	0.0027	0.75 ± 0.0004	3.49 ± 0.08	1805 ± 108	2.04E+10 ± 1.08E+09
1	-	5.24	-	0.318	-	*246.7*	*5.05E+07*
1	-	2.30	-	0.237	-	*3,3684*	-

∗ INGV: istituto nazionale di geofisica e vulcanologia, Sezione di Palermo, Italy.
∗ LFCR: Laboratoire des Fluides Complexes et leurs Réservoirs, Pau, France.
[1]Data from Rizzo et al. (2019)
b.d.l.: below detection limit.
n.m.: not measured.
-: not determined.

Ar as the gas carrier. The uncertainty on the chemical compositions is about 2% of the measured values. Detection limits are 1 ppm for hydrocarbons, 400 ppm for H_2 and, 100 ppm for CO_2, O_2 and N_2. Carbon isotopic measurements were performed on an Agilent 7890A gas chromatograph interfaced to a Thermo Fischer MAT 253 isotope ratio mass spectrometer using a GC-Isolink or a Finigan GC-C III interface using He carrier gas. Uncertainties on $\delta^{13}C\text{-}CO_2$ are ±0.1‰. The He-isotopic compositions were analyzed at the Noble Gas Laboratory at SUERC. Gases were purified and analysed as per previously published procedures (Györe et al., 2015; 2021). The ^4He and ^{20}Ne concentrations and $^3He/^4He$ isotope ratios were measured using a MAP 215–50 mass spectrometer (Williams et al., 2005). For the ^4He and ^{20}Ne contents, uncertainties are ~3% (Table 1). The He-isotopic ratio uncertainties vary from 3.8% to 5.4%.

2 Results

The gases are dominated by N_2, CO_2 and O_2, with concentrations ranging from 28% to 73%, 7%–64% and 6%–20%, respectively (Table 1). Ar was measured on three samples, concentrations varying between 0.69% and 0.89%. H_2 concentration ranges from below the detection limit to 10,100 ppm, while CH_4 exhibits narrower range from 46 to 300 ppm. Other hydrocarbon species (e.g., C_2H_6, C_6^+) and H_2S are below the detection limits. CO was occasionally present in low concentrations, but was considered unreliable due to the sampling procedures and storage, which can release CO and contaminate the samples. The $\delta^{13}C\text{-}CO_2$ range from 0.0‰ vs. PDB to +0.8‰ vs. PDB and the He-isotope composition scales from 1.42 to 2.96 R_a (where R_a is the He atmospheric ratio of 1.39 x 10^{-6}; Sano et al., 1998). ^4He and ^{20}Ne concentrations vary from 5.98 to 9.22 ppm and from 5.77 to 21.51 ppm, respectively. Sample Nea 2 was not analyzed because the low $^4He/^{20}Ne$ ratio implied high atmospheric contamination.

2.1 Discussion

2.1.1 Temporal evolution of atmospheric contamination

The gas samples are characterized by high concentrations of O_2, N_2 and Ar with respect to air values (Table 1), indicating a significant contamination by atmospheric-derived gases. In the $CO_2\text{-}N_2\text{-}O_2$ ternary diagram shown in Figure 3A, the data are on a mixing line between air and a deeper gas that is rich in CO_2. This mixing can occur during sample collection, or may represent air trapped in the fumarolic system. We quantified this contamination and corrected the chemical composition using

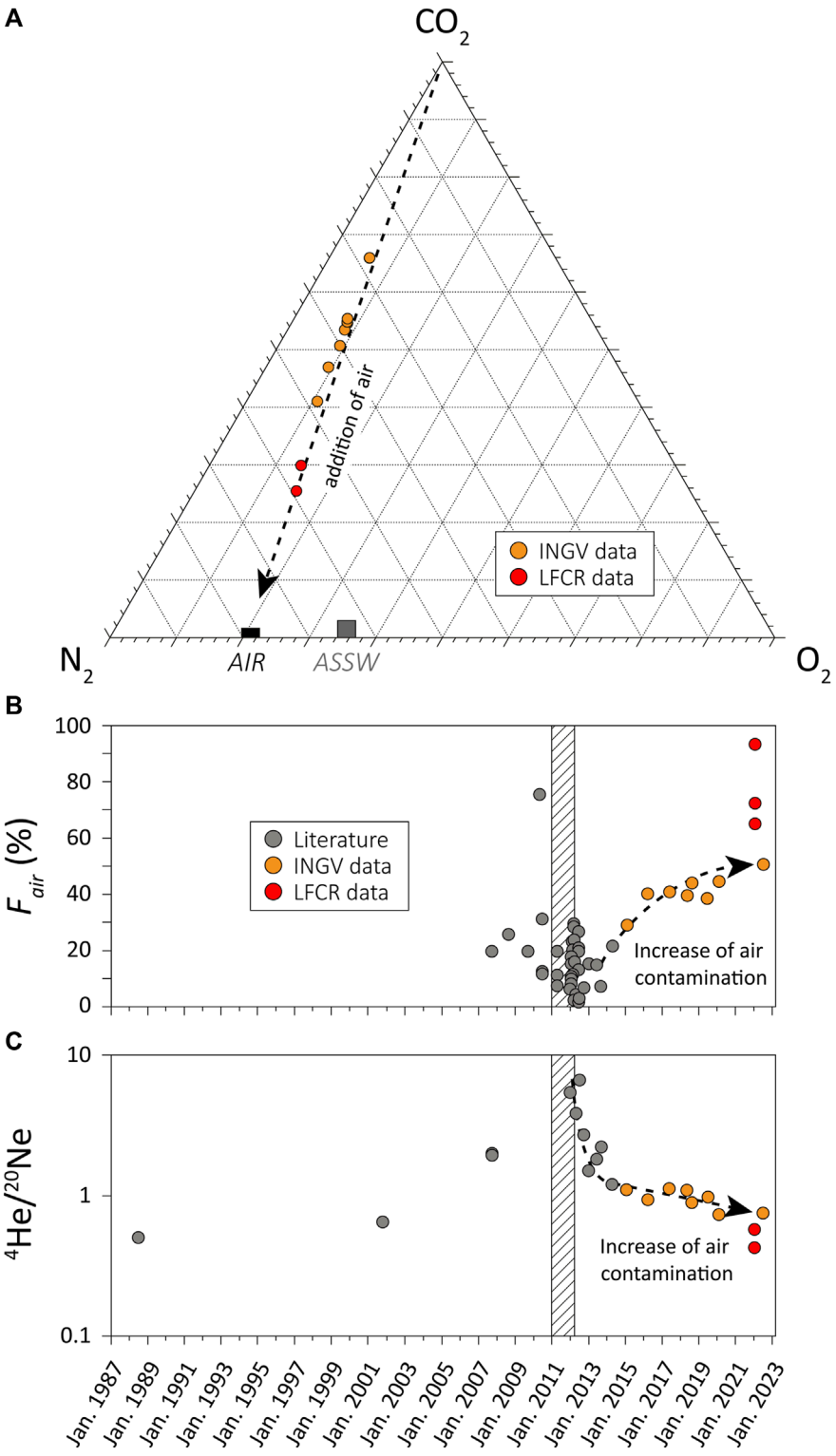

FIGURE 3
(A) CO_2-N_2-O_2 ternary diagram showing the trend of air addition to a deep component rich in CO_2. The ASSW endmember is also reported. **(B)** Temporal evolution of the calculated percentage of atmospheric contamination (F). **(C)** Temporal evolution of the $^4He/^{20}Ne$. The dashed square corresponds to the 2011–2012 period of volcanic unrest at Santorini, modified from Rizzo et al., 2015 and references therein. The trend of increasing air contamination is shown in **(B, C)**. Literature data are from Nagao et al., 1991; Shimizu et al., 2005; D'Alessandro et al., 2010; Tassi et al., 2013; Rizzo et al., 2015.

TABLE 2 Restored chemical composition before addition of atmospheric-derived gases. The percentage of air contamination is also reported, as well as the temperature obtained from H_2/N_2 gas geothermometer, assuming a liquid phase.

ID	Sample	CO_2	N_2 (%)	H_2 (ppm)	CH_4 (ppm)	He (ppm)	F_{air} (%)	Temp. H_2/N_2 geothermometer (°C)
1	NK	90.4%	7.4	14195	421	7.70	28.9	242
2	NK	87.7%	9.2	13508	439	6.54	40.0	235
3	NK	84.4%	9.8	12653	425	7.28	40.8	230
4	NK	85.6%	9.7	11351	436	8.98	39.3	227
5	NK	88.4%	9.8	10614	450	8.54	43.9	225
6	NK	86.6%	10.4	4,588	449	8.09	38.2	196
7	NK	83.4%	15.4	10556	697	11.20	44.6	210
8	Nea 1	92.7%	7.3	1938	469	19.83	72.7	180
9	Nea 2	-	-	-	-	-	93.8	-
10	Nea 3	85.0%	13.7	11203	502	15.81	65.6	215
11	NK	84.2%	16.9	11819	465	6.74	50.7	210

Eqs 1, 2, and by assuming that O_2 was only derived from the atmosphere (Rizzo et al., 2019).

$$[i]_{corrected} = \frac{\left([i]_{sample} - \left([i]_{air} * F\right)\right)}{(1-F)} \quad (1)$$

$$F = \frac{[O_2]_{sample}}{[O_2]_{air}} \quad (2)$$

These equations enabled calculation of the concentration of a species denoted by *i*, before air addition in the system (i.e., $[i]_{corrected}$). $[i]_{sample}$, $[i]_{air}$, $[O_2]_{sample}$ and $[O_2]_{air}$ represent the concentration of this species *i* and the O_2 content, in the sample and in air, respectively. *F* is the fraction of atmospheric-derived gases (expressed in %). Corrected chemical compositions are presented in Table 2. The results show that CO_2, N_2, H_2 and CH_4 were the main components before addition of air in the system. An uncertainty in the correction must be considered because some O_2 consumption may have occurred before gas emission at the surface.

Noble gas samples are also affected by atmospheric contamination, as shown by the low values of the $^4He/^{20}Ne$ ratio (Table 1; Porcelli et al., 2002). We corrected the He content and isotopic ratio (i.e., R/R_a) by using Eqs 1–3, respectively (Craig et al., 1978).

$$\frac{R_c}{R_a} = \frac{\left(\left(\frac{R}{R_a}\right)_{sample} * \left(\frac{^4He}{^{20}Ne}\right)_{sample} - \left(\frac{^4He}{^{20}Ne}\right)_{air}\right)}{\left(\left(\frac{^4He}{^{20}Ne}\right)_{sample} - \left(\frac{^4He}{^{20}Ne}\right)_{air}\right)} \quad (3)$$

The He isotopic ratio corrected for contamination by atmospheric-derived component $\left(\text{i.e.,}\frac{R_c}{R_a}\right)$ is obtained by using the ratio of the sample $\left(\text{i.e.,}\left(\frac{R}{R_a}\right)_{sample}\right)$ and the $\frac{^4He}{^{20}Ne}$ ratios in the sample and in air (i.e., $\left(\frac{^4He}{^{20}Ne}\right)_{sample}$; $\left(\frac{^4He}{^{20}Ne}\right)_{air} = 0.318$).

The low concentration of CO_2 in air (Table 1), compared to the deep source identified in Figure 3A implies that atmospheric contamination has a small or negligible impact on the measured C-isotope composition ($\delta^{13}C\text{-}CO_2$), even if the fraction of atmospheric-derived gases is important in the sample. This isotopic ratio has therefore not been corrected.

Figures 3B, C show the temporal evolution of *F*, the fraction of air in the reactive gas samples, and the $^4He/^{20}Ne$ used to study the contamination by atmosphere in the noble gas samples. Figure 3B shows that the proportion of air in the gas mixture has tended to increase continuously since the end of the 2011–2012 unrest. This is also evident in Figure 3C in which the $^4He/^{20}Ne$ decreases over the same period, indicating an input of atmospheric-derived ^{20}Ne compared to the deep-radiogenic ^4He. As most of the data from the literature and the 2015–2022 samples from the INVG come from the same fumaroles (NK), we can assume that this increase in air contamination is unrelated to the sampling. In addition, the samples were taken at different periods each year. The possibility of meteorological control seems unlikely, as it should result in random variations rather than the general trend observed over several years. We can therefore infer that air-derived gas is present in the subsurface. As the samples are admixtures between atmosphere and volcanic/hydrothermal sources, the contribution of the latter is becoming decreasingly important. The self-sealing process of the channels that carry the deep gas upwards or the opening of air circulation conduits could be the cause of these temporal anomalies. Nevertheless, the possibility of a lowered flux of magmatic/hydrothermal gases seems the most likely explanation.

2.1.2 Geochemical monitoring of the fumarolic activity between 2015 and 2022

In volcanic systems with a well-developed hydrothermal system, periods of quiescence and unrest are tracked by CO_2/CH_4 (Chiodini, 2009 and references therein). Increases of CO_2/CH_4 are usually attributed to CO_2 exsolution from a magmatic body and it generally reflects periods of unrest during which the melt is depressurized. Figure 4A shows the temporal evolution of the CO_2/CH_4 ratio for the fumaroles of Nea Kameni. From July 2010 to March 2012, a significant increase of this ratio was interpreted as due to the upwelling of new and poorly degassed magma (Rizzo et al., 2015). After this event, in mid-2012, the volcano regained stability, with CO_2/CH_4 attaining a value that is similar to the pre-unrest period. Since then no significant anomalies were recorded and our chemical data from 2015 to 2022 follows the same trend than the one measured after the volcanic unrest.

N_2 concentrations corrected for atmospheric contamination are plotted over time in Figure 4B. Similarly, when compared to the CO_2/CH_4 ratio evolution from July 2010 to March 2012, the N_2 concentration has dramatically increased, with the highest values reached in July 2010 (up to 55%). The N_2 is derived either from subducted sediment where it is fixed as NH_4^+ or from the mantle (Sano et al., 2001; Barry and Hilton, 2016). The similarity between the high N_2 content and the 2011–2012 unrest suggests that the magmatic body was enriched in N_2. This anomaly stopped around March 2012. The deep N_2 concentration has slightly increased over time although an uncertainty in the corrected values must be considered as the fraction of air increased after 2012 (Figure 3B).

The temporal evolution of H_2 concentration for different fumaroles of Nea Kameni are shown in Figure 4C. From March 2011 to February 2012 a sharp increase of H_2 has been detected in a fumarole of Nea Kameni (Tassi et al., 2013). Based on studies of geothermal gas equilibrium (Giggenbach, 1980) and the H_2/H_2O, Tassi et al. (2013) attributed this change to: i) a primary H_2 production by thermal dissociation of H_2O from a heat pulse and ii) a passive enrichment caused by steam condensation at shallow depth. The origin of the heat pulse has been related to a fresh magma injection or increase in rock permeability due to the seismic swarm. The H_2 concentration has significantly decreased after February 2012.

Figure 4D shows the number of earthquakes (M > 1; depth <30 km) inside the caldera (*cf.* Figure 2B for location of the area), represented as cumulative per year since 2008. The only period of intense seismic activity was between October 2011 and February 2012 with few earthquakes recorded since. Moreover, several sources of deflation were reported in the caldera between 2012 and 2017 (Papageorgiou et al., 2019).

Our geochemical data together with the seismic and ground deformation data show that no new magma upwelling has occurred since 2012. Indeed, the low CO_2/CH_4 ratios and non-atmospheric N_2 concentrations record an absence of input of deep gas (i.e., CO_2, N_2) in the system while the low H_2 concentrations suggest the lack of new significant thermal perturbations. Thus, the geochemical signature records the evolution of the magma emplaced during the last unrest.

2.1.3 Origin of CO_2 and He

Figure 5A shows the He isotopic composition of the fumarole gases plotted *versus* the $^4He/^{20}Ne$ ratio. Most data plot on a mixing curve representing a binary admixture between air (or air saturated water) and a magmatic gas having He isotopic ratios between 3.3 and 3.9 R_a. This overlaps the He isotope ratios measured in phenocryst olivines from mafic enclaves (3.0–3.6 R_a) include in the 1,570–1,573 and 1925–1928 dacitic lavas of Nea Kameni (Rizzo et al., 2015) and implies that the fumaroles are directly tapping magmatic volatiles. This contrasts with the higher $^3He/^4He$ measured in submarine thermal springs from the northern part of the Santorini caldera (6.6 R_a) and at the Kolumbo seamounts (7.1 R_a) (Carey et al., 2013; Rizzo et al., 2016; Moreira et al., 2019) (Figure 5A). If the Kolumbo fluids truly represent the magmatic $^3He/^4He$, the lower values of the Nea Kameni fluids imply there is a contribution from either ^4He-rich fluid in the hydrothermal plumbing system or assimilation of metamorphic basement by the magma that feeds the Nea Kameni hydrothermal system (Rizzo et al., 2015).

$CO_2/^3He$ and $\delta^{13}C\text{-}CO_2$ are used to constraint the source of CO_2 (Marty and Jambon, 1987; Sano and Marty, 1995). $CO_2/^3He$ and $\delta^{13}C\text{-}CO_2$ seems to track a binary mixing between a limestone ($CO_2/^3He = 1x10^{13}$; $\delta^{13}C\text{-}CO_2 = 0‰$) and a mantle ($CO_2/^3He = 2x10^9$; $\delta^{13}C\text{-}CO_2 = -4‰$) endmember (Figure 5B). It could imply that the CO_2 emitted at Nea Kameni is largely derived from limestones either from the subduction of carbonate-rich sediments and/or assimilation of the carbonate basement (Rizzo et al., 2015). If we consider that the gases from Kolumbo and Santorini have a common mantle origin in terms of CO_2 and He, then the Kolumbo gases shows that the CO_2 prior to its dissolution in water has likely a more pronounced mantle signature ($CO_2/^3He = \sim1.26x10^{10}$; $\delta^{13}C\text{-}CO_2 = \sim$-0.4‰) than CO_2 discharged at Nea Kameni fumaroles ($CO_2/^3He > \sim1.84x10^{10}$), as with He, although with some chemical and $\delta^{13}C\text{-}CO_2$ fractionation ($CO_2/^3He = 9.71x10^9$-$3.34x10^{10}$; $\delta^{13}C\text{-}CO_2 = -0.87‰$–$0.80‰$) that we assume to be due to gas-water interaction before emission (Rizzo et al., 2019) (Figure 5B).

2.1.4 Temporal evolution of He concentration controlled by gas-water interactions

Figure 6A shows the temporal evolution of He isotopic ratio corrected for atmospheric contamination (R_c/R_a) for the fumarolic gases of Nea Kameni. The He-isotope composition of volcanic gases records the ascent and degassing of new volatile-rich magmas (Caracausi et al., 2003; Rizzo et al., 2006; 2009; 2015; 2019; Nuccio et al., 2008; Boudoire et al., 2020; Torres-González et al., 2020; Sandoval-Velasquez et al., 2023). This phenomenon was observed at Santorini during the last unrest, when $^3He/^4He$ increased from 3.62 R_a in October 2007 to 3.94 R_a in January 2012 (Rizzo et al., 2015). After this event the He isotopic ratio has decreased albeit showing fluctuations (3.3–3.9 R_a). The origin of the variation is not clear but given the low and uniform CO_2/CH_4 ratios, H_2 concentrations and the lack of significant seismic activity inside the caldera (Figures 4A–C), we exclude the upwelling of new batches of magma.

The long-term variation of He concentration of the fumarolic gases of Nea Kameni is shown in Figure 6B. It was relatively low between 1988 and 2007, but increased from September 2009 to January 2012. In May 2012, He concentrations dropped back to lower values and since then gradually increased, until July 2022

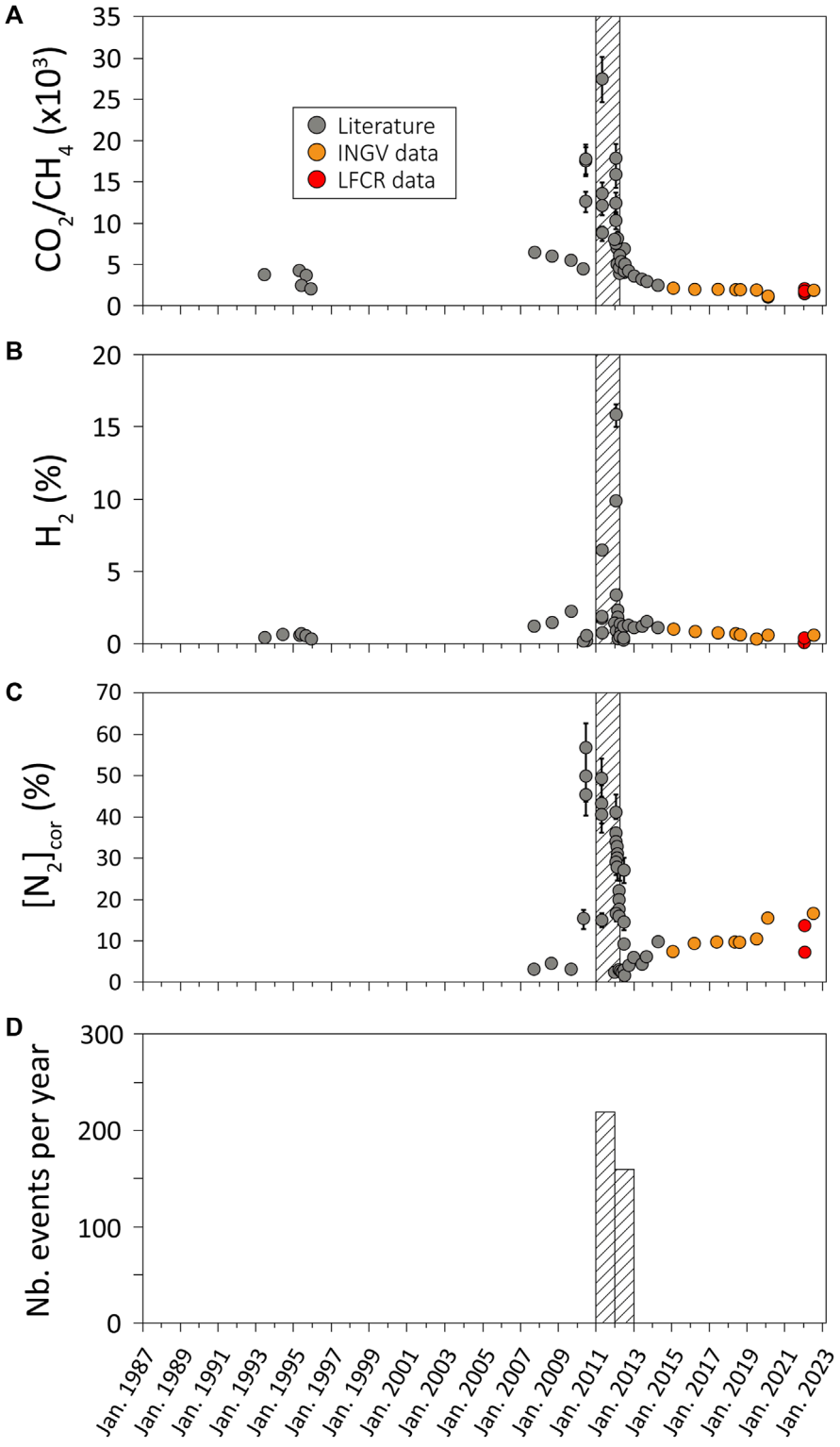

FIGURE 4
Temporal evolution of Nea Kameni fumarolic major gases, as well as seismic activity inside the caldera. **(A)** CO_2/CH_4 ratio (x10^3). **(B)** H_2 concentration. **(C)** N_2 concentration corrected for air contamination. The dashed square corresponds to the 2011–2012 period of volcanic unrest at Santorini, modified from Rizzo et al., 2015 and references therein. Literature data are from Chiodini, 1998; D'Alessandro et al., 2010; Tassi et al., 2013; Rizzo et al., 2015. **(D)** Cumulative number of earthquakes per year, recorded inside the caldera of Santorini (*cf.* Figure 2B). Data from bbnet.gein.noa.gr.

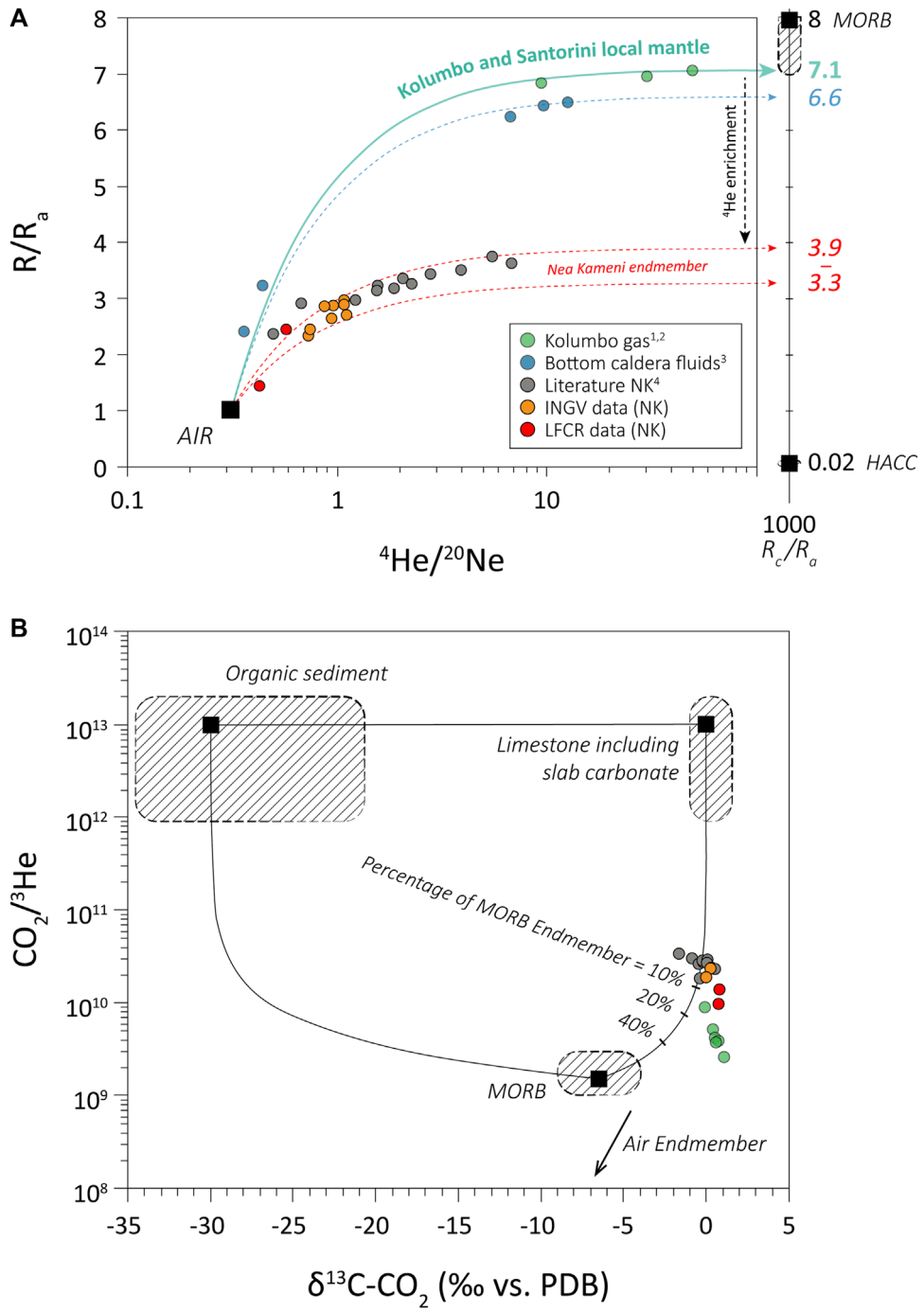

FIGURE 5
Plots showing the origin of He and CO_2 in the gas samples from the Christiana-Santorini-Kolumbo Volcanic Field, respectively. **(A)** Mixing diagram showing the He isotopic ratio reported against the $^4He/^{20}Ne$. Endmembers are from Kurz and Jenkins, 1981. HACC: Hypothetical Aegean Continental Crust. Literature data are from [4]Nagao et al., 1991; [4]Shimizu et al., 2005; [4]D'Alessandro et al., 2010; [1]Carey et al., 2013; [4]Rizzo et al., 2015; [3]Moreira et al., 2019; [2]Rizzo et al., 2019. **(B)** $CO_2/^3He$ ratio *versus* $\delta^{13}C$-CO_2 for fumarole gases. Mantle-limestone mixing uses compositions from Marty and Jambon, 1987; Javoy and Pineau, 1991; Sano and Marty, 1995. Literature data are from [4]D'Alessandro et al., 2010; [4]Rizzo et al., 2015; [2]Rizzo et al., 2019. The black curves show the binary mixing between the different sources of CO_2. Uncertainties are smaller than the size of the data points. Samples with a $^4He/^{20}Ne$ ratio lower than the air ratio of 0.318 were not plotted.

when a slight drop occurred again. Given the low He content in the air (5.24 ppm), the increase in atmospheric contamination cannot explain the increase in He concentrations observed. This trend is anti-correlated with the $CO_2/^3He$ ratio (Figures 6B, C). For instance, during 2011–2012 the high He content and the low $CO_2/^3He$ were also accompanied by higher $^3He/^4He$ and CO_2/CH_4 values that appear to be consistent with the arrival of magmatic fluids (Figures 4A, 6A–C). As the increase of He

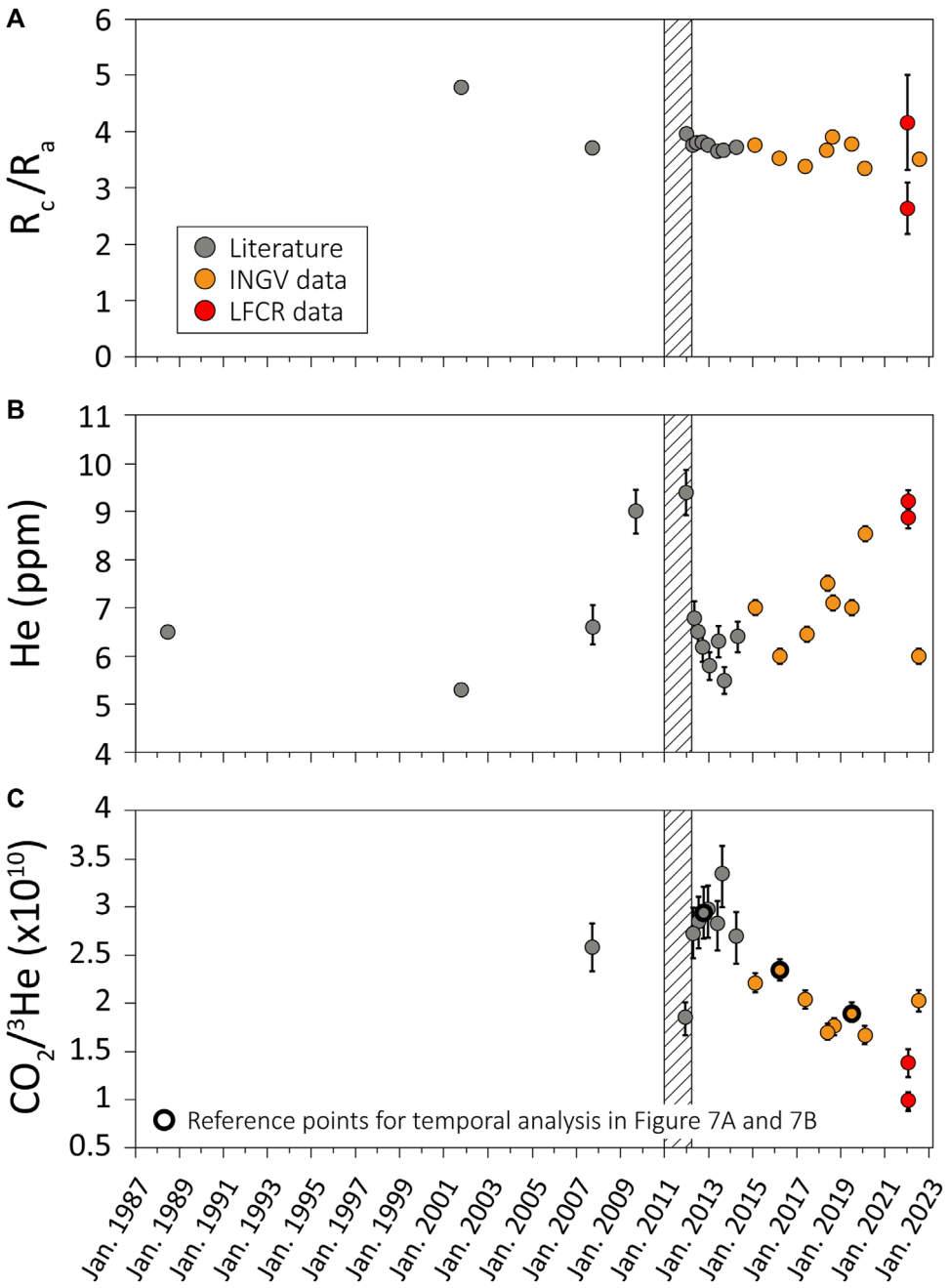

FIGURE 6
Temporal evolution of He and CO_2 concentration in the fumarolic gases of Nea Kameni. **(A)** Corrected He isotopic ratio R_c/R_a, **(B)** He concentration, and **(C)** $CO_2/^3He$. The dashed square corresponds to the 2011–2012 period of volcanic unrest at Santorini, modified from Rizzo et al., 2015 and references therein. Literature data are from Nagao et al., 1991; Shimizu et al., 2005; D'Alessandro et al., 2010; Rizzo et al., 2015.

concentration after 2011–2012 unrest is not linked to magma recharge, we suggest that the decoupling between He and CO_2 is due to a preferential dissolution of CO_2 as the magmatic gases rise to the surface through the aquifer (Rizzo et al., 2019). This can strongly impact the chemical composition of fluids (e.g., He concentration, CO_2/CH_4, $CO_2/^3He$ values) (Rizzo et al., 2019). In addition, the CO_2 dissolution may also fractionate the carbon isotope composition ($\delta^{13}C$-CO_2) at some pH and temperature conditions (Clark and Fritz, 1997).

2.1.5 Model of CO_2 dissolution in water

Selective gas dissolution in water has been modeled at variable temperatures (25°C–374°C) using a similar approach as the one presented in Rizzo et al. (2019). We use this model to calculate the theorical composition curve of the residual CO_2 ($CO_2/^3He$ vs. $\delta^{13}C$-CO_2), once this gas preferentially dissolves in water. We have varied the boundary conditions, such as temperature, pH and initial bulk composition to fit the dissolution curves on our data and discuss the reasons of the temporal decrease of the $CO_2/^3He$ ratio (*cf.* section

"Constraints on the hydrothermal temperature and variations of the gas-water equilibrium conditions"). We made this model by representing a condensation process under equilibrium condition. We have considered an open-system in which the gas-saturated parcels of water were continuously removed. The $CO_2/^3He$ ratio has been corrected by using Eq. 4 (Rayleigh, 1896):

$$\frac{R_v}{R_{v_0}} = f^{\alpha-1} \tag{4}$$

where R_v is the ratio of interest (i.e., He/CO_2), in the residual gas phase, R_{v_0} is the initial bulk ratio which has to be hypothesized (i.e., residual gas fraction = 1), f is the residual gas fraction that we vary from 0 to 1 and α is the fractionation factor determined by the solubility ratio between the two species considered (i.e., k_{H-CO_2}/k_{H-He}). The Henry solubility constants were determined at high temperature by using the equations presented by Fernandez-Prini et al. (2003) and Harvey (1996). These equations require the calculation of the saturated vapor pressure which has been calculated by using the equation presented in Wagner and Pruss (1993). To transform the instantaneous, He/CO_2 in the residual gas phase to the $CO_2/^3He$, we used the average R_c/R_a value recorded over our period of study (~3.6 R_a).

As explained above, the CO_2 dissolution also affects the C-isotope composition in the residual gas phase. To correct for this effect, we used Eq. 5, presented in Clark and Fritz (1997):

$$\delta^{13}C - CO_2 = \left(\delta^{13}C - CO_2\right)_0 + \varepsilon \ln(f) \tag{5}$$

where $\delta^{13}C - CO_2$ is the C-isotope composition in the residual gas phase, $\left(\delta^{13}C - CO_2\right)_0$ is the initial C isotopic ratio, ε is the fractionation factor between DIC and gaseous CO_2 and f is the same fraction of residual gas as the one presented previously. To calculate the fractionation factor ε we used Eq. 6, presented in Zhang and Quay, (1995) and Allègre, (2008):

$$\varepsilon_{DIC-CO_2(g)} = \frac{[H_2CO_3]\varepsilon_{H_2CO_3-CO_2(g)} + [HCO_3^-]\varepsilon_{HCO_3^--CO_2(g)} + [CO_3^{2-}]\varepsilon_{CO_3^{2-}-CO_2(g)}}{[H_2CO_3] + [HCO_3^-] + [CO_3^{2-}]} \tag{6}$$

The isotopic fractionation between CO_2 (g) and CO_2 (aq) depends on the water temperature and on the molar fraction of the different dissolved organic carbon species (i.e., H_2CO_3, HCO_3^- and CO_3^{2-}), which is directly correlated to the pH of the solvent that we varied. Each single fractionation factor was determined at high temperature by using the equation presented in Zhang and Quay, (1995).

2.1.6 Constraints on the hydrothermal temperature and variations of the gas-water equilibrium conditions

We used the geothermometric functions based on the CO/CO_2 and H_2/N_2 ratios (Tarchini et al., 2019 and references therein) to estimate the hydrothermal temperature over our survey period (Table 2). As CO was considered unreliable in our samples, we assumed a liquid phase and adopted the same $FeO\text{-}FeO_{1.5}$ hydrothermal gas buffer than previously used at Nea Kameni by Tarchini et al., 2019. The H_2/N_2 geothermometer track the ammonia dissociation and we therefore based our calculations on the concentrations obtained after atmospheric correction (Table 2). The results presented in Table 2 suggest a decrease of the hydrothermal temperature between 2015 and 2022 (i.e., from ~260°C to ~196°C).

We attempt to observe this temperature variations through the C-He isotope compositions. As discussed earlier, the decrease of the $CO_2/^3He$ ratio over time is related to the process of preferential CO_2 dissolution in water compared to He, rather than CO_2 and He source changes or increase of air contamination. We thus assume that the initial/pristine $CO_2/^3He$ and $\delta^{13}C\text{-}CO_2$ values do not change significantly over time, as present values reflect a low level of magmatic activity comparable to pre-2011 unrest. To construct our models of CO_2 dissolution presented in Figures 7A, B, we assume that this pristine CO_2 composition lies on a Limestone-MORB binary mixing curve (Sano and Marty, 1995). We use the hydrothermal temperature estimate (~260°C in a liquid phase) determined by the CO/CO_2 and H_2/N_2 geothermometric functions in October 2012 to approximate the pH-dependent initial compositions (Figures 7A, B; Tarchini et al., 2019).

In the first model presented in Figure 7A, we use a constant pH of 5 (measured and assumed in the gas-water interaction model at Kolumbo; Rizzo et al., 2019) and vary the gas/water equilibrium temperature to fit the C-He isotope compositions measured in April 2016 and July 2019. The theoretical CO_2 dissolution curves are calculated for gas/water equilibrium temperatures of 260°C, 195°C, 100°C and 25°C. We highlight that at this pH value, the variability in the $CO_2/^3He$ and $\delta^{13}C\text{-}CO_2$ values could be explained by a temperature decrease through time. This temperature decrease favors the CO_2 dissolution, as shown by the decrease of the residual gas fraction over time. However, temperature estimates based on this model are unrealistic knowing that surface fumarolic gases are at least 90°C.

In the plot of Figure 7B we use a second model that considers a fixed temperature range between 260°C and 195°C, as estimated in 2012 and 2019 from the H_2/N_2 geothermometer. Assuming the different pH-dependent initial compositions, we calculate the corresponding CO_2 dissolution curves for pH values of 8, 6 and 4. The results show that for all the pH values in this range, the C-He isotope data fit with a possible decrease of the hydrothermal temperature. These temporal variations in gas/water equilibrium temperature could also be accompanied by a drop in the pH of the water but it seems unlikely over this period of few years. The plot in Figure 7B also highlights that there is no way of fitting the gas/water equilibrium temperatures in 2012 and 2019 with the estimates given by the H_2/N_2 geothermometer if we assume a pristine composition on the Limestone-MORB binary mixing curve (having a curvature coefficient R of 1). This may imply that: i) the H_2/N_2 geothermometer and the CO_2 dissolution model do not trace the same temperatures within the hydrothermal system, due, e.g., to a multistep vertically-elongated system; ii) the temporal increase in air contamination compromises the temperature estimations given by the H_2/N_2 geothermometer; iii) the composition of CO_2 before dissolution is characterized by a lower $\delta^{13}C\text{-}CO_2$ and a higher $CO_2/^3He$ than the values hypothesized in our models (*cf.* Figure 7B). The latter hypothesis could more easily explain some of the literature data, which seem to define a trend toward the organic sediment endmember (*cf.* Figure 5B). These C-He isotope compositions (obtained in 2013) could then be explained by slight variations in equilibrium conditions, rather than a source change.

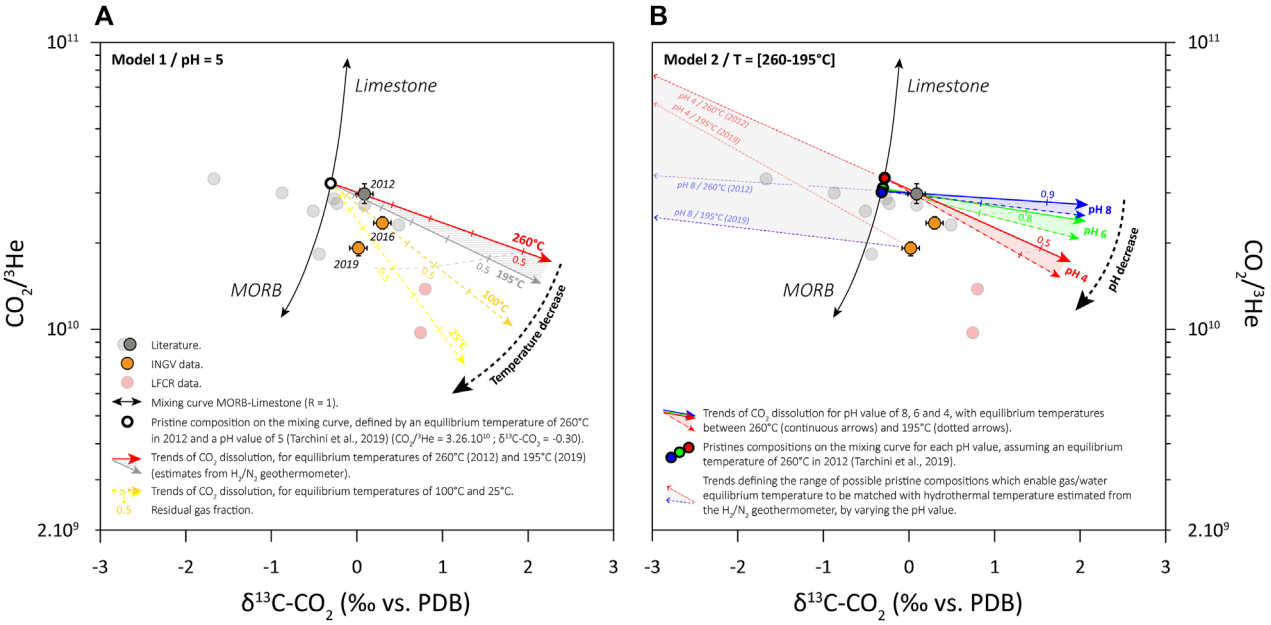

FIGURE 7
Plot of $CO_2/^3He$ *versus* the $\delta^{13}C$-CO_2 showing binary mixing between asthenosphere mantle and limestone (Marty and Jambon, 1987; Javoy and Pineau, 1991; Sano and Marty, 1995). The path of selective gas dissolution in water, modeled by an open-system condensation process under equilibrium conditions are represented for different pristine CO_2 compositions, equilibrium temperatures and pH of the water. Litterature data are from D'Alessandro et al., 2010; Rizzo et al., 2015. **(A)** Model 1 of CO_2 dissolution in water at pH = 5 and equilibrium temperatures of 260°C, 195°C, 100°C and 25°C. **(B)** Model two of CO_2 dissolution in water for pH values of 4, 6 and 8, assuming a range of temperature between 260°C and 195°C (estimated from the H_2/N_2 gas geothermometer in 2012 and 2019).

The results obtained from the H_2/N_2 geothermometer and the CO_2 dissolution models predict decreases of the hydrothermal temperature over the period 2015–2022, which is consistent with the absence of recharge of the magmatic reservoir. It is nevertheless important to note that other parameters such as the equilibrium pressure, the salinity of the water or the gas-water volumetric ratio are not considered in the models. They may have an impact on the chemical and isotope compositions. However, there are no thermodynamic approaches that include these parameters for calculating the evolution of the $\delta^{13}C$-CO_2 during CO_2 dissolution at high temperature and it is thus impossible to quantify their effects.

3 Conclusion

The major gas and C-He isotope composition of fumarole gases at Nea Kameni sampled between 2015 and 2022 record the quiescent state of the Santorini volcano. Unlike the 2011–2012 unrest, this period is characterized by low CO_2/CH_4 and $N_{2cor.}$ concentrations that reflect the lack of input of new magmatic volatiles. Low H_2 concentrations suggest that there were no new heat pulses, and, in addition, seismic activity inside the caldera has remained low over the survey period. The atmospheric contribution to the gases tends to increase with time consistent with a decrease of the deep gas flux. Helium isotopic ratios show slight fluctuation without a clear temporal trend.

The gradual increase in He concentration coupled to a $CO_2/^3He$ decrease is due to enhanced dissolution of deep CO_2 in groundwater that can be modeled using open-system Rayleigh fractionation. The chemical and C-isotope compositions for the preferential CO_2 dissolution show that the temporal decrease of the $CO_2/^3He$ ratio can be explained by a decrease of the hydrothermal temperature, which is also observed using gas geothermometry. These observations highlight the gas depletion and cooling of the magma emplaced at ~4 km depth during the last volcanic unrest of 2011–2012. This is consistent with the geodetic post-unrest response and the deflation measured between 2012 and 2017 by Papageorgiou et al. (2019).

Data availability statement

The original contributions presented in the study are included in the article/Supplementary material, further inquiries can be directed to the corresponding author.

Author contributions

AlB: Conceptualization, Data curation, Formal Analysis, Investigation, Methodology, Project administration, Supervision, Validation, Visualization, Writing–original draft, Writing–review and editing. AnB: Conceptualization, Funding acquisition, Investigation, Methodology, Project administration, Supervision, Validation, Visualization, Writing–review and editing. AR: Conceptualization, Data curation, Investigation, Methodology, Resources, Supervision, Visualization, Writing–review and editing. UB: Data curation, Investigation, Methodology, Writing–review

and editing. DG: Investigation, Methodology, Writing–review and editing. WD'A: Data curation, Investigation, Methodology, Resources, Writing–review and editing. J-PC: Investigation, Project administration, Supervision, Writing–review and editing. KK: Data curation, Investigation, Methodology, Resources, Writing–review and editing. MP: Funding acquisition, Writing–review and editing.

Funding

The author(s) declare that financial support was received for the research, authorship, and/or publication of this article. The authors recieved a financial support from the ORIGAMI partnership chair. This chair is co-funded by Total E&P Recherche et Développement, presently TotalEnergies/OneTech and by E2S-UPPA (Solutions pour l'Energie et l'Environnement), implying CNRS (Centre National de la Recherche Scientifique) and UPPA (Université de Pau et des Pays de l'Adour).

Acknowledgments

Isomass Scientific Inc. is the distributor of analytical instruments used in this research. Isomass Scientific Inc. receives no direct benefit from the publication of this work. Thanks to the ORIGAMI partnership chair - by UPPA-E2S and TotalEnergies for funding this study. We sincerely thank Ygor Oliveri, Francesco Salerno and Mariano Tantillo for their contributions to the data. Thank you to the municipality of Thira and the people of the tourist boats for the access to the Nea Kameni island. Many thanks to Finlay M. Stuart, Guillaume Galliero, Nicolas Beaudoin and Benjamin Lefeuvre for their help. Finally, we thank the Frontiers in Earth Science team, the reviewers and the editors (Marco Viccaro, Yuri Taran, Marco Moretti) for their contributions to this project.

Conflict of interest

Author DG was employed by Isomass Scientific Inc.

The remaining authors declare that the research was conducted in the absence of any commercial or financial relationships that could be construed as a potential conflict of interest.

Publisher's note

References

Allègre, C. J. (2008). *Isotope geology*. Cambridge: Cambridge University Press. doi:10.1017/CBO9780511809323

Barberi, F., and Carapezza, M. L. (1994). Helium and CO2 soil gas emission from Santorini (Greece). *Bull. Volc.* 56, 335–342. doi:10.1007/BF00326460

Barry, P. H., and Hilton, D. R. (2016). Release of subducted sedimentary nitrogen throughout Earth's mantle. *Geochem. Perspect. Lett.* 2 (2), 148–159. doi:10.7185/geochemlet.1615

Biryol, C. B., Beck, S. L., Zandt, G., and Özacar, A. A. (2011). Segmented African lithosphere beneath the Anatolian region inferred from teleseismic P-wave tomography. *Geophys. J. Int.* 184, 1037–1057. doi:10.1111/j.1365-246X.2010.04910.x

Bocchini, G. M., Brüstle, A., Becker, D., Meier, T., Van Keken, P. E., Ruscic, M., et al. (2018). Tearing, segmentation, and backstepping of subduction in the Aegean: new insights from seismicity. *Tectonophysics* 734-735, 96–118. doi:10.1016/j.tecto.2018.04.002

Bohnhoff, M., Rische, M., Meier, T., Becker, D., Stavrakakis, G., and Harjes, H. P. (2006). Microseismic activity in the hellenic Volcanic Arc, Greece, with emphasis on the seismotectonic setting of the santorini–amorgos zone. *Tectonophysics* 423 (1-4), 17–33. doi:10.1016/j.tecto.2006.03.024

Bond, A., and Sparks, R. S. J. (1976). The minoan eruption of Santorini, Greece. *J. Geol. Soc. Lond.* 132, 1–16. doi:10.1144/gsjgs.132.1.0001

Boudoire, G., Rizzo, A. L., Arienzo, I., and Di Muro, A. (2020). Paroxysmal eruptions tracked by variations of helium isotopes: inferences from Piton de la Fournaise (La Réunion island). *Sci. Rep.* 10, 9809. doi:10.1038/s41598-020-66260-x

Bountzouklis, C. (2016). "Monitoring of Santorini (Greece) volcano during post-unrest period (2014-2016) with interferometric time series of sentinel-1A," in *Student thesis series INES. Physical geography and ecosystem science* (Sweden: Lund University).

Budetta, G., Condarelli, D., Fytikas, M., Kolios, N., Pascale, G., Rapolla, A., et al. (1984). Geophysical prospecting on the Santorini islands. *Bull. Volcanol.* 47, 447–466. doi:10.1007/BF01961218

Caliro, S., Chiodini, G., and Paonita, A. (2014). Geochemical evidences of magma dynamics at Campi Flegrei (Italy). *Geochim. Cosmochim. Acta* 132, 1–15. doi:10.1016/j.gca.2014.01.021

Cantner, K., Carey, S., and Nomikou, P. (2014). Integrated volcanologic and petrologic analysis of the 1650 AD eruption of Kolumbo submarine volcano, Greece. *J. Volcanol.* 269, 28–43. doi:10.1016/j.jvolgeores.2013.10.004

Caracausi, A., Favara, R., Giammanco, S., Italiano, F., Paonita, A., Pecoraino, G., et al. (2003). Mount Etna: geochemical signals of magma ascent and unusually extensive plumbing system. *Geophys. Res. Lett.* 30 (2). doi:10.1029/2002GL015463

Carey, S., Nomikou, P., Croff Bell, K., Lilley, M., Lupton, J., Roman, C., et al. (2013). CO2 degassing from hydrothermal vents at Kolumbo submarine volcano, Greece, and the accumulation of acidic crater water. *J. Geol.* 41, 1035–1038. doi:10.1130/G34286.1

Chiodini, G., Cioni, R., Di Paola, G. M., Dotsika, E., Fytikas, M., and Guidi, M. (1998). "Geochemistry of Santorini fluids," in Proceedings of the 2nd Workshop, The European laboratory volcanoes, Santorini, Greece, EUR 18161 EN, eds R. Editor R. Casale, M. Fytikas, G. Sigvaldasson, and G. E. Vougioukalakis (Luxembourg: European Commission), 193–232.

Chiodini, G. (2009). CO2/CH4 ratio in fumaroles a powerful tool to detect magma degassing episodes at quiescent volcanoes. *Geophys. Res. Lett.* 36. doi:10.1029/2008GL036347

Clark, I. D., and Fritz, P. (1997). *Environmental isotopes in hydrogeology*. Boca Raton, FL: CRC Press, 328.

Craig, H. (1957). The natural distribution of radiocarbon and the exchange time of carbon dioxide between atmosphere and sea. *Tellus* 9 (1), 1–17. doi:10.3402/tellusa.v9i1.9078

Craig, H., Lupton, J. E., Welhan, J. A., and Poreda, R. (1978). Helium isotope ratios in Yellowstone and Lassen Park volcanic gases. *Geophys. Res. Lett.* 5, 897–900. doi:10.1029/GL005i011p00897

D'Alessandro, W., Brusca, L., Martelli, M., Rizzo, A. L., and Kyriakopoulos, K. (2010). Geochemical characterization of natural gas manifestations in Greece. *Bull. Geol. Soc. Greece* 43 (5), 2327–2337. doi:10.12681/bgsg.11633

Daskalopoulou, K. (2017). *Geochemistry of gas manifestations in Greece*, Doctoral dissertation. Palermo, Italy: Università degli Studi di Palermo (Italy), National and Kapodistrian University of Athens (Greece), Istituto Nazionale di Geofisica e Vulcanologia.

Daskalopoulou, K., Calabrese, S., Grassa, F., Kyriakopoulos, K., Parello, F., Tassi, F., et al. (2018). Origin of methane and light hydrocarbons in natural fluid

emissions: a key study from Greece. *Chem. Geol.* 479, 286–301. doi:10.1016/j.chemgeo.2018.01.027

Dimitriadis, I., Karagianni, E., Panagiotopoulos, D., Papazachos, C., Hatzidimitriou, P., Bohnhoff, M., et al. (2009). Seismicity and active tectonics at Coloumbo Reef (Aegean Sea, Greece): monitoring an active volcano at Santorini volcanic center using a temporary seismic network. *Tectonophysics* 465, 136–149. doi:10.1016/j.tecto.2008.11.005

Dimitriadis, I., Papazachos, C., Panagiotopoulos, D., Hatzidimitriou, P., Bohnhoff, M., Rische, M., et al. (2010). P and S velocity structures of the Santorini–Coloumbo volcanic system (Aegean Sea, Greece) obtained by non-linear inversion of travel times and its tectonic implications. *J. Volcanol.* 195, 13–30. doi:10.1016/j.jvolgeores.2010.05.013

Druitt, T. H., Costa, F., Deloule, E., Dungan, M., and Scaillet, B. (2012). Decadal to monthly timescales of magma transfer and reservoir growth at a caldera volcano. *Nature* 482, 77–80. doi:10.1038/nature10706

Druitt, T. H., Edwards, L., Mellors, R. M., Pyle, D. M., Sparks, R. S. J., Lanphere, M., et al. (1999). Santorini volcano. *Geol. Soc. Mem.* 19, 165.

Druitt, T. H., Mellors, R. A., Pyle, D. M., and Sparks, R. S. J. (1989). Explosive volcanism on Santorini, Greece. *Geol. Mag.* 126, 95–126. doi:10.1017/S0016756800006270

Druitt, T. H., Pyle, D. M., and Mather, T. A. (2019). Santorini volcano and its plumbing system. *Elements* 15, 177–184. doi:10.2138/gselements.15.3.177

European Marine Observation and Data Network (EMODnet) (2024). EMODnet map viewer. Available at: www.emodnet.eu.

Fernández-Prini, R., Alvarez, J. L., and Harvey, A. H. (2003). Henry's constants and vapor–liquid distribution constants for gaseous solutes in H2O and D2O at high temperatures. *J. Phys. Chem. Ref. Data* 32, 903–916. doi:10.1063/1.1564818

Feuillet, N. (2013). The 2011–2012 unrest at Santorini rift: stress interaction between active faulting and volcanism. *Geophys. Res. Lett.* 40, 3532–3537. doi:10.1002/grl.50516

Flaherty, T., Druitt, T. H., Francalanci, L., Schiano, P., and Sigmarsson, O. (2022). Temporal variations in the diversity of primitive melts supplied to the Santorini silicic magmatic system and links to lithospheric stresses. *Contrib. Mineral. Petrol.* 177 (8), 79. doi:10.1007/s00410-022-01941-6

Fouqué, F. A. (1879). "Santorin et ses éruptions," in *Libraire de L'Académie de Médecine*, 440.

Francalanci, L., Vougioukalakis, G. E., Perini, G., and Manetti, P. (2005). A West-East traverse along the magmatism of the South Aegean volcanic arc in the light of volcanological, chemical and isotope data. *Dev. Volcanol.* 7, 65–111. doi:10.1016/S1871-644X(05)80033-6

Francalanci, L., and Zellmer, G. F. (2019). Magma genesis at the South Aegean volcanic arc. *Elements* 15, 165–170. doi:10.2138/gselements.15.3.165

Fytikas, M., Innocenti, F., Manetti, P., Peccerillo, A., Mazzuoli, R., and Villari, L. (1984). Tertiary to Quaternary evolution of volcanism in the Aegean region. *J. Geol. Soc. Lond.* 17, 687–699. doi:10.1144/GSL.SP.1984.017.01.55

Georgalas, G. C. (1953). L'éruption du volcan de Santorin en 1950. *Bull. Volcanol.* 13 (1), 39–55. doi:10.1007/bf02596790

Giggenbach, W. F. (1980). Geothermal gas equilibria. *Geochim. Cosmochim. Acta* 44, 2021–2032. doi:10.1016/0016-7037(80)90200-8

Grigoriadis, V. N., Tziavos, I. N., Tsokas, G. N., and Stampolidis, A. (2016). Gravity data inversion for Moho depth modeling in the Hellenic area. *Pure Appl. Geophys.* 173, 1223–1241. doi:10.1007/s00024-015-1174-y

Györe, D., Pujol, M., Gilfillan, S. M., and Stuart, F. M. (2021). Noble gases constrain the origin, age and fate of CO2 in the vaca muerta shale in the neuquén basin (Argentina). *Chem. Geol.* 577, 120294. doi:10.1016/j.chemgeo.2021.120294

Györe, D., Stuart, F. M., Gilfillan, S. M. V., and Waldron, S. (2015). Tracing injected CO2 in the Cranfield enhanced oil recovery field (MS, USA) using He, Ne and Ar isotopes. *Int. J. Greenh. Gas. Control* 42, 554–561. doi:10.1016/j.ijggc.2015.09.009

Hansen, S. E., Evangelidis, C. P., and Papadopoulos, G. A. (2019). Imaging slab detachment within the Western Hellenic subduction zone. *Geochem. Geophys. Geosystems* 20, 895–912. doi:10.1029/2018GC007810

Harvey, A. H. (1996). Semiempirical correlation for Henry's constants over large temperature ranges. *AIChE J.* 42 (5), 1491–1494. doi:10.1002/aic.690420531

Heath, B. A., Hooft, E. E. E., Toomey, D. R., Papazachos, C. B., Nomikou, P., Paulatto, M., et al. (2019). Tectonism and its relation to magmatism around Santorini volcano from upper crustal P wave velocity. *J. Geophys. Res. Solid Earth* 124, 10610–10629. doi:10.1029/2019JB017699

Hellenic seismological broadband network (NOA_HL) (2024). Catalogue of revised locations. Institute of geodynamics, national observatory of athens (NOA). Available at: http://bbnet.gein.noa.gr.

Hooft, E. E. E., Heath, B. A., Toomey, D. R., Paulatto, M., Papazachos, C. B., Nomikou, P., et al. (2019). Seismic imaging of Santorini: subsurface constraints on caldera collapse and present-day magma recharge. *Earth Planet. Sci. Lett.* 514, 48–61. doi:10.1016/j.epsl.2019.02.033

Javoy, M., and Pineau, F. (1991). The volatiles record of a "popping" rock from the Mid-Atlantic Ridge at 14°N: chemical and isotopic composition of gas trapped in the vesicles. *Earth Planet. Sci. Lett.* 107 (3-4), 598–611. doi:10.1016/0012-821X(91)90104-P

Jolivet, L., and Brun, J. P. (2010). Cenozoic geodynamic evolution of the Aegean. *Int. J. Earth Sci.* 99, 109–138. doi:10.1007/s00531-008-0366-4

Jolivet, L., Faccenna, C., Huet, B., Labrousse, L., Le Pourhiet, L., Lacombe, O., et al. (2013). Aegean tectonics: strain localisation, slab tearing and trench retreat. *Tectonophysics* 597-598, 1–33. doi:10.1016/j.tecto.2012.06.011

Jolivet, L., Menant, A., Sternai, P., Rabillard, A., Arbaret, L., Augier, R., et al. (2015). The geological signature of a slab tear below the Aegean. *Tectonophysics* 659, 166–182. doi:10.1016/j.tecto.2015.08.004

Klaver, M., Carey, S., Nomikou, P., Smet, I., Godelitsas, A., and Vroon, P. (2016). A distinct source and differentiation history for Kolumbo submarine volcano, Santorini volcanic field, Aegean arc. *Geochem. Geophys. Geosystems* 17, 3254–3273. doi:10.1002/2016GC006398

Kurz, M. D., and Jenkins, W. J. (1981). The distribution of helium in oceanic basalt glasses. *Earth Planet. Sci. Lett.* 53 (1), 41–54. doi:10.1016/0012-821X(81)90024-8

Lagios, E., Sakkas, V., Novali, F., Bellotti, F., Ferretti, A., Vlachou, K., et al. (2013). SqueeSAR and GPS ground deformation monitoring of Santorini volcano (1992–2012): tectonic implications. *Tectonophysics* 594, 38–59. doi:10.1016/j.tecto.2013.03.012

Le Pichon, X., and Angelier, J. (1979). The Hellenic arc and trench system: a key to the neotectonic evolution of the eastern Mediterranean area. *Tectonophysics* 60, 1–42. doi:10.1016/0040-1951(79)90131-8

Lion, A. (2018). *Thermochronologic and geochronologic investigations of the pre-volcanic crystalline basement of Thera (Santorini), Greece: determining the tectonostratigraphy and deformational history of the metamorphic core*. Doctoral dissertation. Canada: University of Ottawa.

Martin, V. M., Morgan, D. J., Jerram, D. A., Caddick, M. J., Prior, D. J., and Davidson, J. P. (2008). Bang! Month-scale eruption triggering at Santorini volcano. *Science* 321, 1178. doi:10.1126/science.1159584

Marty, B., and Jambon, A. (1987). C/3He in volatile fluxes from the solid Earth: implications for carbon geodynamics. *Earth Planet. Sci. Lett.* 83 (1-4), 16–26. doi:10.1016/0012-821X(87)90047-1

McVey, B. G., Hooft, E. E. E., Heath, B. A., Toomey, D. R., Paulatto, M., Morgan, J. V., et al. (2020). Magma accumulation beneath Santorini volcano, Greece, from P-wave tomography. *Geology* 48, 231–235. doi:10.1130/G47127.1

Moreira, M., Escartin, J., Scelin, L., Ruzié-Hamilton, L., Nomikou, P., Mével, C., et al. (2019). New insights into the plumbing system of Santorini using Helium and Carbon isotopes. *Geochem. Perspect. Lett.* 10, 46–50. doi:10.7185/geochemlet.1914

Nagao, K., Kita, I., Matsuda, J., and Mitropoulos, P. (1991). Noble gas isotope geochemistry of volcanic gases from the Aegean island arc. *Bull. Geol. Soc. Greece* 15 (2), 33–41.

Newman, A. V., Stiros, S., Feng, L., Psimoulis, P., Moschas, F., Saltogianni, V., et al. (2012). Recent geodetic unrest at Santorini caldera, Greece. *Geophys. Res. Lett.* 39 (6). doi:10.1029/2012GL051286

Nomikou, P., Hübscher, C., and Carey, S. (2019). The christiana–santorini–kolumbo volcanic field. *Elements* 15, 171–176. doi:10.2138/gselements.15.3.171

Nomikou, P., Hübscher, C., Papanikolaou, D., Farangitakis, G. P., Ruhnau, M., and Lampridou, D. (2018). Expanding extension, subsidence and lateral segmentation within the Santorini - amorgos basins during Quaternary: implications for the 1956 Amorgos events, central - south Aegean Sea, Greece. *Tectonophysics* 722, 138–153. doi:10.1016/j.tecto.2017.10.016

Nomikou, P., Parks, M. M., Papanikolaou, D., Pyle, D. M., Mather, T. A., Carey, S., et al. (2014). The emergence and growth of a submarine volcano: the Kameni islands, Santorini (Greece). *GeoResJ* 1, 8–18. doi:10.1016/j.grj.2014.02.002

Nuccio, P. M., Paonita, A., Rizzo, A. L., and Rosciglione, A. (2008). Elemental and isotope covariation of noble gases in mineral phases from Etnean volcanics erupted during 2001–2005, and genetic relation with peripheral gas discharges. *Earth Planet. Sci. Lett.* 272 (3-4), 683–690. doi:10.1016/j.epsl.2008.06.007

Pank, K., Hansteen, T. H., Geldmacher, J., Hauff, F., Jicha, B., Nomikou, P., et al. (2022). Mineralogy and geochemistry of lavas from the submarine lower caldera walls of Santorini Volcano (Greece). *J. Volcanol.* 427, 107556. doi:10.1016/j.jvolgeores.2022.107556

Paonita, A., Caracausi, A., Iacono-Marziano, G., Martelli, M., and Rizzo, A. L. (2012). Geochemical evidence for mixing between fluids exsolved at different depths in the magmatic system of Mt Etna (Italy). *Geochim. Cosmochim. Acta* 84, 380–394. doi:10.1016/j.gca.2012.01.028

Papadimitriou, P., Kapetanidis, V., Karakonstantis, A., Kaviris, G., Voulgaris, N., and Makropoulos, K. (2015). The Santorini volcanic complex: a detailed multi-parameter seismological approach with emphasis on the 2011–2012 unrest period. *J. Geodyn.* 85, 32–57. doi:10.1016/j.jog.2014.12.004

Papageorgiou, E., Foumelis, M., and Parcharidis, I. (2012). Long-and short-term deformation monitoring of Santorini volcano: unrest evidence by DInSAR

analysis. *IEEE J. Sel. Top. Appl. Earth Observations Remote Sens.* 5, 1531–1537. doi:10.1109/JSTARS.2012.2198871

Papageorgiou, E., Foumelis, M., Trasatti, E., Ventura, G., Raucoules, D., and Mouratidis, A. (2019). Multi-sensor SAR geodetic imaging and modelling of Santorini volcano post-unrest response. *Remote Sens.* 11 (3), 259. doi:10.3390/rs11030259

Papoutsis, I., Papanikolaou, X., Floyd, M., Ji, K. H., Kontoes, C., Paradissis, D., et al. (2013). Mapping inflation at Santorini volcano, Greece, using GPS and InSAR. *Geophys. Res. Lett.* 40, 267–272. doi:10.1029/2012GL054137

Parks, M. M., Biggs, J., England, P., Mather, T. A., Nomikou, P., Palamartchouk, K., et al. (2012). Evolution of Santorini volcano dominated by episodic and rapid fluxes of melt from depth. *Nat. Geosci.* 5, 749–754. doi:10.1038/ngeo1562

Parks, M. M., Caliro, S., Chiodini, G., Pyle, D. M., Mather, T. A., Berlo, K., et al. (2013). Distinguishing contributions to diffuse CO2 emissions in volcanic areas from magmatic degassing and thermal decarbonation using soil gas 222Rn–δ13C systematics: application to Santorini volcano, Greece. *Earth Planet. Sci. Lett.* 377-378, 180–190. doi:10.1016/j.epsl.2013.06.046

Parks, M. M., Moore, J. D., Papanikolaou, X., Biggs, J., Mather, T. A., Pyle, D. M., et al. (2015). From quiescence to unrest: 20 years of satellite geodetic measurements at Santorini volcano, Greece. *J. Geophys. Res. Solid Earth* 120 (2), 1309–1328. doi:10.1002/2014JB011540

Pfeiffer, T. (2001). Vent development during the Minoan eruption (1640 BC) of Santorini, Greece, as suggested by ballistic blocks. *J. Volcanol.* 106 (3-4), 229–242. doi:10.1016/S0377-0273(00)00273-0

Piromallo, C., and Morelli, A. (2003). P wave tomography of the mantle under the Alpine-Mediterranean area. *J. Geophys. Res. Solid Earth* 108 (B2), 2065. doi:10.1029/2002JB001757

Porcelli, D., Ballentine, C. J., and Wieler, R. (2002). "An overview of noble gas geochemistry and cosmochemistry," in *Noble gases in geochemistry and cosmochemistry. Rev. Mineral. Geochem.* (Berlin, Germany: De Gruyter).

Preine, J., Karstens, J., Hübscher, C., Nomikou, P., Schmid, F., Crutchley, G. J., et al. (2022). Spatio-temporal evolution of the christiana-santorini-kolumbo volcanic field, Aegean Sea. *Geology* 50, 96–100. doi:10.1130/G49167.1

Pyle, D. M., and Elliott, J. R. (2006). Quantitative morphology, recent evolution, and future activity of the Kameni Islands volcano, Santorini, Greece. *Geosphere* 2 (5), 253–268. doi:10.1130/GES00028.1

Rayleigh, L. (1896). L. *Theoretical considerations respecting the separation of gases by diffusion and similar processes. Lond. Edinb. Dublin Philos. Mag. J. Sci.* 42 (259), 493–498. doi:10.1080/14786449608620944

Rizzo, A. L., Barberi, F., Carapezza, M. L., Di Piazza, A., Francalanci, L., Sortino, F., et al. (2015). New mafic magma refilling a quiescent volcano: evidence from He-Ne-Ar isotopes during the 2011-2012 unrest at Santorini, Greece. *Geochem. Geophys. Geosystems* 16, 798–814. doi:10.1002/2014GC005653

Rizzo, A. L., Caracausi, A., Chavagnac, V., Nomikou, P., Polymenakou, P. N., Mandalakis, M., et al. (2016). Kolumbo submarine volcano (Greece): an active window into the Aegean subduction system. *Sci. Rep.* 6 (1), 28013. doi:10.1038/srep28013

Rizzo, A. L., Caracausi, A., Chavagnac, V., Nomikou, P., Polymenakou, P. N., Mandalakis, M., et al. (2019). Geochemistry of CO2-rich gases venting from submarine volcanism: the case of Kolumbo (Hellenic Volcanic Arc, Greece). *Front. Earth Sci.* 7, 60. doi:10.3389/feart.2019.00060

Rizzo, A. L., Caracausi, A., Favara, R., Martelli, M., Paonita, A., Paternoster, M., et al. (2006). New insights into magma dynamics during last two eruptions of Mount Etna as inferred by geochemical monitoring from 2002 to 2005. *Geochem. Geophys. Geosystems* 7 (6), 1–12. doi:10.1029/2005GC001175

Rizzo, A. L., Grassa, F., Inguaggiato, S., Liotta, M., Longo, M., Madonia, P., et al. (2009). Geochemical evaluation of observed changes in volcanic activity during the 2007 eruption at Stromboli (Italy). *J. Volcanol.* 182 (3-4), 246–254. doi:10.1016/j.jvolgeores.2008.08.004

Rosi, M., Acocella, V., Cioni, R., Bianco, F., Costa, A., De Martino, P., et al. (2022). Defining the pre-eruptive states of active volcanoes for improving eruption forecasting. *Front. Earth Sci.* 10, 795700. doi:10.3389/feart.2022.795700

Sachpazi, M., Laigle, M., Charalampakis, M., Diaz, J., Kissling, E., Gesret, A., et al. (2016). Segmented Hellenic slab rollback driving Aegean deformation and seismicity. *Geophys. Res. Lett.* 43, 651–658. doi:10.1002/2015GL066818

Sandoval-Velasquez, A., Rizzo, A. L., Casetta, F., Ntaflos, T., Aiuppa, A., Alonso, M., et al. (2023). The noble gas signature of the 2021 Tajogaite eruption (La Palma, Canary Islands). *J. Volcanol.* 443, 107928. doi:10.1016/j.jvolgeores.2023.107928

Sano, Y., and Marty, B. (1995). Origin of carbon in fumarolic gas from island arcs. *Chem. Geol.* 119 (1-4), 265–274. doi:10.1016/0009-2541(94)00097-R

Sano, Y., Takahata, N., Nishio, Y., Fischer, T. P., and Williams, S. N. (2001). Volcanic flux of nitrogen from the earth. *Chem. Geol.* 171, 263–271. doi:10.1016/S0009-2541(00)00252-7

Sano, Y., Wakita, H., and Sheng, X. (1988). Atmospheric helium isotope ratio. *Geochem. J.* 22 (4), 177–181. doi:10.2343/geochemj.22.177

Shimizu, A., Sumino, H., Nagao, K., Notsu, K., and Mitropoulos, P. (2005). Variation in noble gas isotopic composition of gas samples from the Aegean arc, Greece. *J. Volcanol.* 140, 321–339. doi:10.1016/j.jvolgeores.2004.08.016

Stiros, S. C., Psimoulis, P., Vougioukalakis, G., and Fyticas, M. (2010). Geodetic evidence and modeling of a slow, small-scale inflation episode in the Thera (Santorini) volcano caldera, Aegean Sea. *Tectonophysics* 494 (3-4), 180–190. doi:10.1016/j.tecto.2010.09.015

Tarchini, L., Carapezza, M. L., Ranaldi, M., Sortino, F., Gattuso, A., and Acocella, V. (2019). Fluid geochemistry contribution to the interpretation of the 2011–2012 unrest of Santorini, Greece, in the frame of the dynamics of the Aegean volcanic arc. *Tectonics* 38, 1033–1049. doi:10.1029/2018TC005377

Tassi, F., Vaselli, O., Papazachos, C. B., Giannini, L., Chiodini, G., Vougioukalakis, G. E., et al. (2013). Geochemical and isotopic changes in the fumarolic and submerged gas discharges during the 2011–2012 unrest at Santorini caldera (Greece). *Bull. Volcanol.* 75 (4), 711. doi:10.1007/s00445-013-0711-8

Torres-González, P. A., Luengo-Oroz, N., Lamolda, H., D'Alessandro, W., Albert, H., Iribarren, I., et al. (2020). Unrest signals after 46 years of quiescence at cumbre vieja, La palma, canary islands. *J. Volcanol.* 392, 106757. doi:10.1016/j.jvolgeores.2019.106757

Wagner, W., and Pruss, A. (1993). International equations for the saturation properties of ordinary water substance. Revised according to the international temperature scale of 1990. Addendum to J. Phys. Chem. Ref. Data **16**, 893 (1987). *J. Phys. Chem. Ref. Data* 22 (3), 783–787. doi:10.1063/1.555926

Williams, A. J., Stuart, F. M., Day, S. J., and Phillips, W. (2005). Using pyroxene microphenocrysts to determine cosmogenic 3He concentrations in old volcanic rocks: an example of landscape development in central Gran Canaria. *Quat. Sci. Rev.* 24, 211–222. doi:10.1016/j.quascirev.2004.07.004

Zhang, J., Quay, P. D., and Wilbur, D. (1995). Carbon isotope fractionation during gas-water exchange and dissolution of CO2. *Geochim. Cosmochim. Acta* 59 (1), 107–114. doi:10.1016/0016-7037(95)91550-D